Chapter 2
Observation of the Post-Ionization Optical Coupling in N_2^+ Lasing in Intense Laser Fields

Yao Fu, Helong Li, Siqi Wang, Erik Lötstedt, Toshiaki Ando, Atsushi Iwasaki, Farhad H. M. Faisal, Kaoru Yamanouchi, and Huailiang Xu

Abstract In this chapter, we introduce our recent studies on the mechanisms responsible for the optical amplification in N_2^+ induced by irradiating nitrogen molecules N_2 with intense laser fields. We demonstrate that the lasing intensities of N_2^+ at 391.4 nm, corresponding to the $B^2\Sigma_u^+$ ($\upsilon = 0$)-$X^2\Sigma_g^+$ ($\upsilon'' = 0$) transition, can be strongly modulated by manipulating the polarization state of the driven laser field, which is ascribed to the post-ionization coupling between the ground $X^2\Sigma_g^+$ state and the first excited $A^2\Pi_u$ state of N_2^+. By using pump-probe methods, we show direct evidences for the optical transition between the $X^2\Sigma_g^+$ and $A^2\Pi_u$ states of N_2^+ in intense laser field, based on which we show the optimization of N_2^+ lasing by designing intense laser fields.

2.1 Introduction

When a powerful femtosecond (fs) laser pulse is externally- or self-focused in pure nitrogen or air, it can induce a variety of dynamical processes of atmospheric constituents [1–4], resulting in electronically and rovibrationally excited atoms, molecules or ions, which are in some cases population-inverted and lead to amplification of the light covering the transitions [5–18]. This type of lasing phenomena in

Y. Fu · H. Li · S. Wang · H. Xu (✉)
State Key Laboratory of Integrated Optoelectronics, College of Electronic Science and Engineering, Jilin University, Changchun 130012, China
e-mail: huailiang@jlu.edu.cn

E. Lötstedt · T. Ando · A. Iwasaki · K. Yamanouchi
Department of Chemistry, School of Science, The University of Tokyo, 7-3-1 Hongo, Bunkyo-ku, Tokyo 113-0033, Japan
e-mail: kaoru@chem.s.u-tokyo.ac.jp

F. H. M. Faisal
Fakultät Für Physik, Universität Bielefeld, 33615 Bielefeld, Germany

H. Xu
CAS Center for Excellence in Ultra-Intense Laser Science, Shanghai 201800, China

K. Yamanouchi et al. (eds.), *Progress in Ultrafast Intense Laser Science XVI*, Topics in Applied Physics 141, https://doi.org/10.1007/978-3-030-75089-3_2

air are popularly called “air lasing”, and have been extensively investigated in recent years because of their high potential in atmospheric applications [16–18]. Recently, lasing in N_2^+ has been paid much attention because it was theoretically predicted that the ionization of N_2, whose ground-state electronic orbital configuration is KK $(\sigma_g 2s)^2(\sigma_u 2s)^2(\pi_u 2p)^4(\sigma_g 2p)^2$, by intense fs laser pulses [19] gives more population on the ground $X^2\Sigma_g{}^+$ state of N_2^+ [20, 21]. As a result, the stimulated amplification of light in the population-inverted N_2^+ could not occur only through the strong-field ionization of N_2. Therefore, considerable effort has been made to interpret the physical origin of the strong-field-induced N_2^+ lasing [22–29].

In 2015, we proposed, as shown in Fig. 2.1, a physical mechanism called “post-ionization optical coupling” to explain the strong-field-induced N_2^+ lasing phenomenon. In this scenario, it was suggested that the ionization of N_2 occurs in the strongest (central) part of the fs laser pulse, and most of N_2^+ cations are prepared in their ground $X^2\Sigma_g{}^+$ state as predicted theoretically. After the ionization, the resultant N_2^+ cations are still within the light field, and thus interact with the rear part of the fs laser pulse, which would induce an optical coupling among the lowest three states of N_2^+, i.e., $X^2\Sigma_g{}^+$, $A^2\Pi_u$ and $B^2\Sigma_u{}^+$, leading to population redistribution in N_2^+, and consequently, the population inversion between the $B^2\Sigma_u{}^+$ and $X^2\Sigma_g{}^+$ states. With this pumping mechanism, it was demonstrated that the population-inverted N_2^+ can be built up very rapidly within a time scale of a few femtoseconds, which agrees well with the experimental observation that N_2^+ lasing can be produced by the excitation of few-cycle 800 nm laser pulses [25].

In this chapter, we present further experimental evidences for the post-ionization coupling mechanism in N_2^+ lasing. We first demonstrate that the intensity (which represents the peak value of the measured signal) of the N_2^+ lasing at 391.4 nm can be significantly enhanced by designing a time-dependent polarized laser field using either the polarization gating (PG) technique [26] or a birefringent crystal [27], which can be convincingly explained by the post-ionization coupling where the modulated driven pulse efficiently transfers the population in the ground $X^2\Sigma_g{}^+$ state to the first

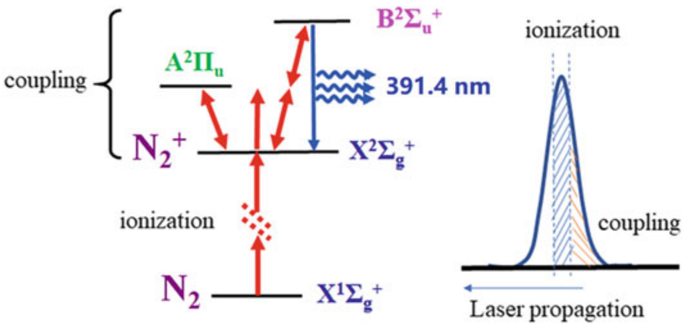

Fig. 2.1 Schematic diagram of post-ionization optical coupling that redistributes the populations among the $X^2\Sigma_g{}^+$, $B^2\Sigma_u{}^+$ and $A^2\Pi_u$ states and establishes the population inversion between the $X^2\Sigma_g{}^+$ and $B^2\Sigma_u{}^+$ states in N_2^+

excited $A^2\Pi_u$ state of N_2^+. This is an “indirect” evidence for the coupling, where the transition between the $X^2\Sigma_g^+$ and $A^2\Pi_u$ states is not directly observed. We then show, using pump-probe methods, the “direct” observations of the optical coupling by introducing an independent coupling pulse to induce the $X^2\Sigma_g^+$-$A^2\Pi_u$ transition, and find that the 391.4 nm lasing intensity can be controlled by modulating the strength, polarization and time delay of the coupling pulse [28, 29]. Based on the deeper understanding of the post-ionization coupling, we achieve the optimization of N_2^+ lasing in an elliptically modulated intense laser field.

2.2 Indirect Observation of $X^2\Sigma_g^+$-$A^2\Pi_u$ Coupling

When the ionization of N_2 occurs at the most intense part of a linearly polarized laser field, the N_2 molecules whose axes are parallel to the polarization direction of the linearly polarized laser field are preferentially ionized [30], and consequently, most of N_2^+ ions are aligned along the polarization direction of the laser field. However, in the post-ionization optical coupling model, the subsequent $X^2\Sigma_g^+$-$A^2\Pi_u$ coupling induced by the rear laser field has the maximum efficiency when the polarization direction of the coupling laser field is perpendicular to the direction of N_2^+ axis because of the perpendicular $X^2\Sigma_g^+$-$A^2\Pi_u$ transition nature of N_2^+ [31]. Therefore, it is expected that the intensity of N_2^+ lasing can be enhanced or reduced if one could control the polarization state of the rear part of the laser pulse. In the following, we will present experimental results of N_2^+ lasing in two types of designed laser fields, whose polarization states in the rear part of the laser pulse change in time, by using the PG technique [26] and birefringent crystal [27].

2.2.1 N_2^+ Lasing Pumped with the Laser Pulse Modulated by the PG Technique

To explore the effect of the laser polarization of the rear part of the pumping laser pulse on N_2^+ lasing, we employ a technique called polarization grating (PG) [32], which is often used in attosecond pulse generation, to modulate the polarization state of the pump laser pulse in time. As shown in Fig. 2.2a, the PG setup used in this study is composed of a 7-order quarter-wave plate (7-QWP) and a 0-order quarter wave plate (0-QWP). The angle between the optical axis of the 7-QWP and the polarization of the input laser pulse is set at 45°, so that the electric field of the laser field modulated by the 7-QWP can be expressed as [26],

$$E_{7-QWP}(t) = \frac{E_0}{\sqrt{2}} g\left(t - \frac{T_{d\_7-QWP}}{2}\right) e_{7-QWP\_o} + \frac{E_0}{\sqrt{2}} g\left(t + \frac{T_{d\_7-QWP}}{2}\right) e_{7-QWP\_e} \quad (2.1)$$

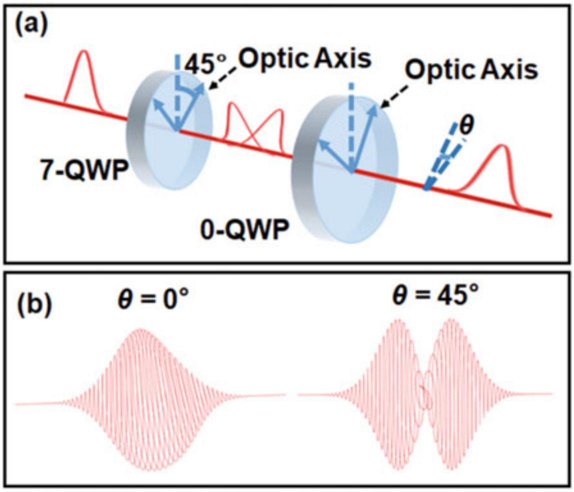

Fig. 2.2 **a** Schematic diagram of the PG, where 7-QWP and 0-QWP represent the 7-order and 0-order quarter wave plates. The angle θ represents the angle between the optical axes of the two quarter wave plates, **b** Amplitudes at $\theta = 0°$ and 45°, respectively

where E_0 is the amplitude of the input laser pulse, and T_{d_7-QWP} is the time delay between the *o* light and the *e* light induced by the 7-QWP with $T_{d\_7-QWP} = 2\pi(7 + 1/4)/\omega$ and $g(t) = e^{-2\ln 2t^2/\tau^2}\sin(\omega t + \varphi)$ is the Gaussian function of the laser pulse, and e_{7-QWP_o} and e_{7-QWP_e} are the unit vectors perpendicular (the *o* light) and parallel (the *e* light) to the optics axis of the 7-QWP, respectively. Then the laser pulse is further modulated by the 0-QWP, with the final electric field expressed as,

$$E_{PG}(t) = \frac{E_0}{\sqrt{2}}\left[g\left(t - \frac{T_{d\_7-QWP} + T_{d\_0-QWP}}{2}\right)*\cos\theta + g\left(t + \frac{T_{d\_7-QWP} - T_{d\_0-QWP}}{2}\right) * \sin\theta\right] e_{0-QWP\_o} + \frac{E_0}{\sqrt{2}}\left[g\left(t - \frac{T_{d\_7-QWP} - T_{d\_0-QWP}}{2}\right)*\sin\theta - g\left(t + \frac{T_{d\_7-QWP} + T_{d\_0-QWP}}{2}\right) * \cos\theta\right] e_{0-QWP\_e} \quad (2.2)$$

where T_{d_0-QWP} is the time delay between the *o* light and the *e* light induced by the 0-QWP with $T_{d\_0-QWP} = (2\pi * (1/4))/\omega$ and e_{0-QWP_o} and e_{0-QWP_e} are the unit vector perpendicular and parallel to the optical axis of the 0-QWP, respectively. It can be seen from (2.2) and Fig. 2.2b that when the angle, θ, between the optical axes of the two wave plates is changed, the polarization state of a linearly polarized pump laser field in the front and rear parts of the laser pulse can be changed from linear to circular or circular to linear, but the polarization state at the peak of the laser pulse (the central part) is kept as linear.

In this study, we carry out the experiments using the linearly polarized output of a Ti:sapphire amplifier (800 nm, 40 fs). After the laser beam passes through the PG, it is focused by a fused silica lens ($f = 40$ cm) into a vacuum chamber filled with pure nitrogen at 10 mbar. N_2^+ lasing is generated by both self- and external-seeding schemes, where self-seeding means that the seed pulse is directly produced by the pump pulse in N_2 gas during propagation, but the external seeding means that the seed pulse is produced by frequency doubling of the pump pulse in a BBO crystal. The forward lasing is collimated by a fused silica lens (f = 30 cm), and recorded by a spectrometer (Andor, Shamrock) equipped with with an ICCD camera (Andor iStar).

With the laser field modulated by the PG with the angle of $\theta = 0°$, where the polarization of the rear part of the laser pulse is linear but its direction changes in time, it can be seen from Fig. 2.3a that the intensity of self-seeding N_2^+ lasing at 391.4 nm (solid line), corresponding to the $B^2\Sigma_u^+(\upsilon = 0)$-$X^2\Sigma_g^+$ $(\upsilon'' = 0)$ transition, can be significantly enhanced when compared with that (dot line) obtained with the pump of the linear polarized light without the PG modulation. For both the cases, the pump laser energies are set at 1.0 mJ. In order to avoid the effect of self-generated seed on the lasing enhancement, we compare the lasing intensities measured in the external seed scheme. In this case, the energies of the pump laser pulses are reduced to 0.6 mJ, so that self-generated seed is negligible. As shown in Fig. 2.3b, the forward N_2^+ lasing produced by the PG-modulated laser pulse (solid line) in the presence of the external seed (dash line) is about one order of magnitude larger than that (dot line) by the linearly polarized laser pulse, which indicates that the population inversion between the $B^2\Sigma_u^+$ and $X^2\Sigma g^+$ states is dramatically changed by the PG-modulated fields.

On the other hand, we also measure the 391.4 nm fluorescence of N_2^+ on the $B^2\Sigma_u^+$-$X^2\Sigma_g^+$ transition by collecting it at a right angle of the laser propagation direction. It is found that the intensity of fluorescence pumped by the PG-modulated laser pulse is slightly weaker than (comparable with) that pumped by the linearly polarized laser pulse (not shown). Since the fluorescence intensity is determined by the population in $B^2\Sigma_u^+$ $(\upsilon = 0)$ state of N_2^+, the enhancement of N_2^+ lasing at 391.4 nm can be thus ascribed to the efficient depletion of the population in the

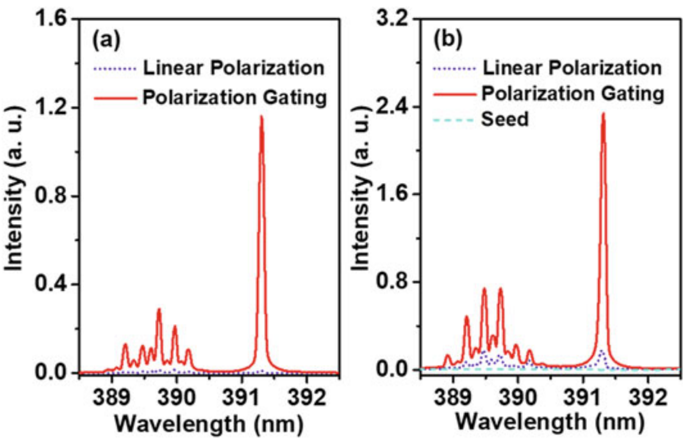

Fig. 2.3 The forward spectra of **a** self-seeding and **b** external seeding N_2^+ lasing obtained by the linearly polarized (dot lines) and PG-modulated (solid lines) laser pulses. The external seed (dash line) is also presented in (**b**). The angle θ is set at $\theta = 0°$

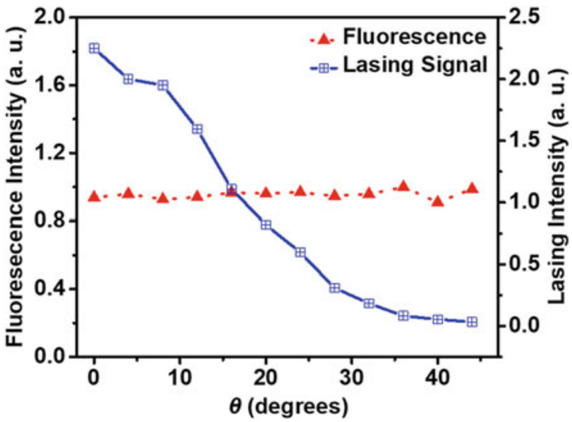

Fig. 2.4 The intensities of the N_2^+ lasing (square) and fluorescence (triangle) obtained with the PG pulse as a function of θ in the range of 0–45°

$X^2\Sigma_g^+(\upsilon" = 0)$ by the optical coupling through the vertical $X^2\Sigma_g^+$-$A^2\Pi_u$ transition, in which the polarization of the coupling field in the rear part of the laser pulse is modulated by the PG.

In particular, it is known from the PG scheme that when we change the angle between the 0-QWP and 7-QWP from $\theta = 0°$ to 45°, the polarization state changes from linear to circular in both the front and rear parts, but the polarization state of the central part of the pulse keeps linear. Because the population in the $B^2\Sigma_u^+$ state is only dependent on the ionization of N_2 by the central part (strongest) of the laser pulse, it is expected that when the angle θ changes from 0° to 45° the fluorescence at 391.4 nm measured from the side direction keeps constant, but the lasing at 391.4 nm, which is dependent on both the populations in the $B^2\Sigma_u^+$ ($\upsilon = 0$) and $X^2\Sigma_g^+$ ($\upsilon" = 0$) states, changes. This is really what we have observed. As shown in Fig. 2.4, when θ changes from 0° to 45°, the intensity of the 391.4 nm fluorescence (triangle) keeps constant in the entire range of θ, but the 391.4 nm lasing (square) decreases monotonously, which can be ascribed to the amplitude of the laser component perpendicular to the N_2^+ axis in the rear laser field decreases from linear polarization to circular polarization, leading to the less $X^2\Sigma_g^+$-$A^2\Pi_u$ perpendicular coupling.

2.2.2 N_2^+ Lasing Pumped with the Laser Pulse Modulated by Multi-order Quarter-Wave Plate

It can be seen from (2.2) that the laser field can be modulated by the PG. In fact, when the laser pulse only passes through the 7-QWP, the amplitude and polarization of the laser pulse can also be modulated as a function of the angle, $\boldsymbol{\alpha}$, between the polarization direction of the linear laser pulse and the fast axis of the 7-QWP, as shown in (2.3), but in this case the polarization state of the central part of the laser pulse changes as well. In this section, we investigate how the lasing behaves in the laser field modulated only by the 7-QWP [27].

$$\boldsymbol{E}(\alpha, t) = E_0 \cos(\alpha) g\left(t - \frac{T_n}{2}\right) e_o + E_0 \sin(\alpha) g\left(t + \frac{T_n}{2}\right) \boldsymbol{e}_e. \quad (2.3)$$

As shown in Fig. 2.5a, the laser field can be separated into two electric field components, the ordinary light (E_y) and the extraordinary (E_x) light, with E_y being parallel to the fast axis of 7-QWP and thus having a larger amplitude at $-45° < \alpha < 45°$ (α represents the angle between the polarization direction of the linearly polarized laser pulse and the fast axis of 7-QWP). Due to the birefringence of the 7-QWP, the two components of the linearly polarized laser pulse will have a time delay of about 20 fs after passing through the 7-QWP, where E_x lags behind E_y. Therefore, in the coupling model [25], the stronger E_y component would induce the ionization of N_2 and the delayed and weaker E_x component would subsequently induce the post-ionization state coupling of N_2^+ through the perpendicular $X^2\Sigma_g^+$-$A^2\Pi_u$ transition. In Fig. 2.5b, we show the integrated intensity of the E_y component ($-\infty < t < \infty$) and that of the E_x component ($0 < t < \infty$) as a function of the angle α between the polarization direction of the linearly polarized laser pulse and the fast axis of 7-QWP.

As a result, we show in Fig. 2.6a the intensity of the N_2^+ lasing at 391.4 nm measured in the external seed scheme as a function of the angle α. The pressure is

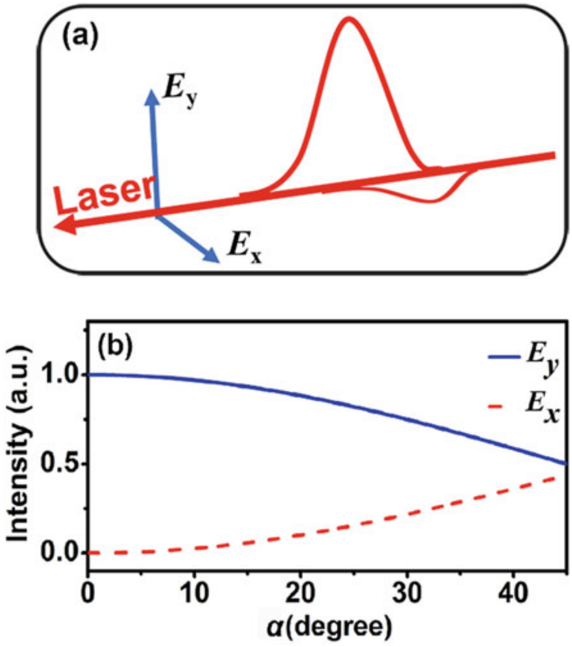

Fig. 2.5 **a** The amplitude of the E_x and E_y components of the laser electric fields with the direction of E_x and E_y perpendicular and parallel to the fast axis (ordinary light axis) of the 7-QWP at $\alpha = 10°$. **b** The intensity of the E_x component, which is proportional to the square of the amplitude, integrated over $0 < t < \infty$ (dash line) and that of E_y integrated over $-\infty < t < \infty$ (solid line) of the laser pulse vary as a function of α

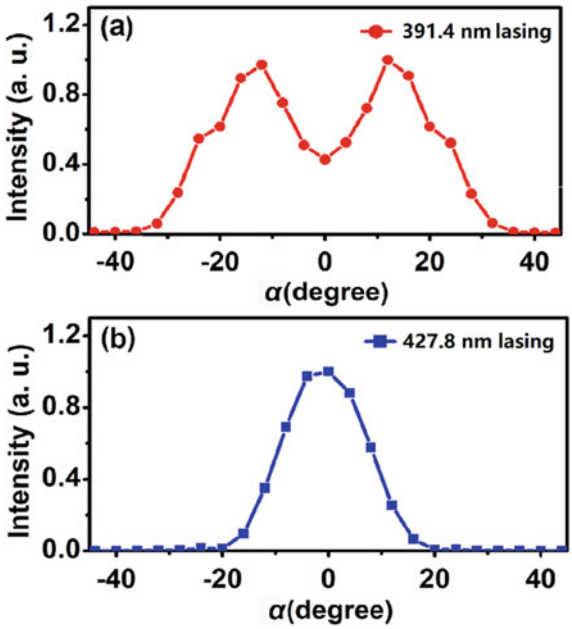

Fig. 2.6 **a** 391.4 nm and **b** 427.8 nm lasing intensity as a function of α in the 7-QWP modulated laser field

10 mbar and the laser energy is 0.7 mJ. It can be seen from Fig. 2.6a that as $|\boldsymbol{\alpha}|$ changes from 0° to 45°, the intensity of the 391.4 nm lasing first increases and then decreases, taking the maximums at the absolute value of α ~ 18°, which may indicate that as the ellipticity of the laser pulse changes there exists a balance between the ionization rate and the coupling efficiency for the population inversion between the $X^2\Sigma_g{}^+(\upsilon'' = 0)$ and $B^2\Sigma_u{}^+(\upsilon = 0)$. That is, as $|\boldsymbol{\alpha}|$ varies from 0° to 45°, E_y decreases, leading to a decreasing ionization probability, and thus less $N_2{}^+$ ions. On the other hand, as $|\boldsymbol{\alpha}|$ changes from 0° to 45°, E_x increases, leading to a stronger coupling field for depleting the population in the $X^2\Sigma_g{}^+(\upsilon'' = 0)$ level through the $X^2\Sigma_g{}^+$-$A^2\Pi_u$ vertical transition after the ionization. Finally, a balance between the ionization and coupling for the population inversion is achieved.

Interestingly, it is found that as $|\boldsymbol{\alpha}|$ changes from 0° to 45°, the intensity of the lasing at 427.8 nm, corresponding to the $B^2\Sigma_u{}^+$ $(\upsilon = 0)$-$X^2\Sigma_g{}^+$ $(\upsilon'' = 1)$ transition, shows different behavior, i.e., monotonically decreasing with the maximum value at α ~ 0° (see Fig. 2.6b). Since the 391.4 and 427.8 nm lasing emissions result from the same upper level $B^2\Sigma_u{}^+$ $(\upsilon = 0)$, the difference in the ellipticity dependences of these two lasing lines may be ascribed to the different variations of the population in the two vibrational levels $\upsilon'' = 0$ and $\upsilon'' = 1$ of the $X^2\Sigma_g{}^+$ state. In fact, it was previously demonstrated that the population in the $X^2\Sigma_g{}^+(\upsilon'' = 1)$ level is very small after ionization [33]. Therefore, the population in the $X^2\Sigma_g{}^+(\upsilon'' = 1)$ level could not be depleted further by the E_x(t) component after the ionization, so that the 427.8 nm lasing is not sensitive to the $X^2\Sigma_g{}^+$-$A^2\Pi_u$ coupling, leading to the result that the 427.8 nm lasing decreases monotonically due to the decreasing ionization probability as $|\boldsymbol{\alpha}|$ changes from 0° to 45°.

To verify the above conjecture on the ellipticity dependences of N_2^+ lasing, we perform numerical simulation of the population distribution of N_2^+ in a multi-order QWP modulated laser field based on the post-ionization optical coupling model [27]. We examine the final difference of the population between the $B^2\Sigma_u^+$ ($\upsilon = 0$) and $X^2\Sigma_g^+$ ($\upsilon'' = 0$) levels and that between $B^2\Sigma_u^+$ ($\upsilon = 0$) and $X^2\Sigma_g^+$ ($\upsilon'' = 1$) levels, as a function of the angle α, and find that for the 427.8 nm transition, the population difference exhibits a maximum at $\alpha = 0°$ and it decreases monotonically as $|\boldsymbol{\alpha}|$ increases, while for the 391.4 nm transition, the maximum values are located at the two symmetric positions of $0° < |\boldsymbol{\alpha}| < 45°$ with a dip at $\alpha = 0°$. These results are in good agreement with the experimental data shown in Fig. 2.6.

2.3 Direct Observation of $X^2\Sigma_g^+$-$A^2\Pi_u$ Coupling

We have demonstrated in Sect. 2.2 that the lasing intensities of N_2^+ can be significantly enhanced or reduced by modulating the polarization of the pump laser pulse, and that the ellipticity dependences of two lasing lines at 391.4 and 427.8 nm can be well explained by the post-ionization coupling among the $X^2\Sigma_g^+$, $A^2\Pi_u$, and $B^2\Sigma_u^+$ states of N_2^+. However, in the above-mentioned polarization modulation methods, both the stronger electric field component used for the ionization of N_2, and the weaker one used as the post-ionization coupling are from the same pump laser pulse, so that the ionization and coupling are entangled within the laser pulse and cannot be well separated and manipulated. Therefore, it would be helpful to provide deeper insight into the coupling mechanism if one could directly show the coupling effect by pump-probe methods, in which the coupling process can be independently operated without disturbing the ionization process. In the following, we will present experimental results for direct observation and manipulation of the coupling in N_2^+ lasing using pump-probe methods [28, 29].

2.3.1 Pump-Coupling-Probe Scheme

Here we design a pump-coupling-probe scheme (see Fig. 2.7), in which we employ an intense 800 nm pump laser pulse (40 fs, 700 μJ) to induce the ionization of N_2, a weak 800 nm laser pulse (40 fs, 20–200 μJ) to manipulate the $X^2\Sigma_g^+$ ($\upsilon'' = 0$)-$A^2\Pi_u$ ($\upsilon' = 2$) coupling of N_2^+, and then a much weaker 400 nm broadband pulse (40 ~ 60 fs, 50 nJ) to externally seed the N_2^+ gain medium [28]. Since the perpendicular $X^2\Sigma_g^+$-$A^2\Pi_u$ transition is sensitive to the polarization direction of the coupling field, it is expected that when we change the polarization direction of the coupling field with respect to that of the pump laser pulse, the population in the $X^2\Sigma_g^+$ ($\upsilon'' = 0$)

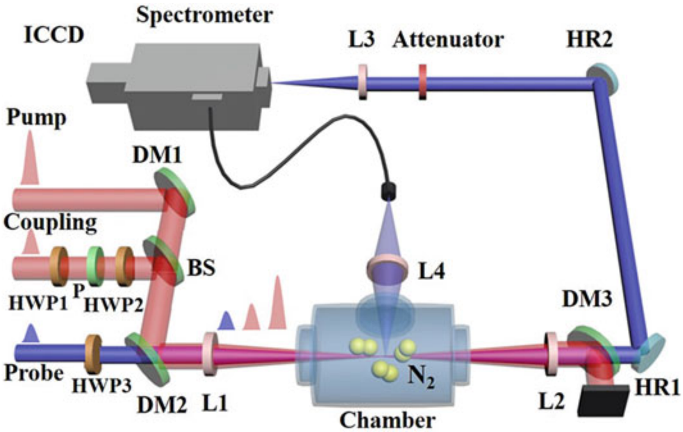

Fig. 2.7 Schematic diagram of the pump-coupling-probe experimental setup. HWP: half-wave plate (1, 2: for 800 nm; 3: for 400 nm); P: polarizer; DM: dichromic mirror; BS: beam splitter; L: fused silica lens (1: $f = 40$ cm; 2: $f = 30$ cm; 3: $f = 6$ cm; 4: $f = 6$ cm); F: filter; HR1 and HR2: 400 nm high reflection mirror

can be depleted to some extent accordingly, and thus the 391.4 nm lasing intensity can be modulated.

In this experiment [28], the delay time between the pump and the coupling pulses, and that between the pump and the seed pulses are set at 70 fs and 200 fs, respectively. With the delay time of 70 fs, the molecular axis of N_2^+ ions prepared along the polarization direction of the pump pulse will not change much after the ionization, and the interference effect between the pump and coupling fields can be negligible because these two pulses (40 fs) are almost separated completely. Figure 2.8 shows the intensity of the 391.4 nm lasing as a function of the angle β between the polarization directions of the pump and the coupling pulses. $\beta = 0°$ and 90° mean that

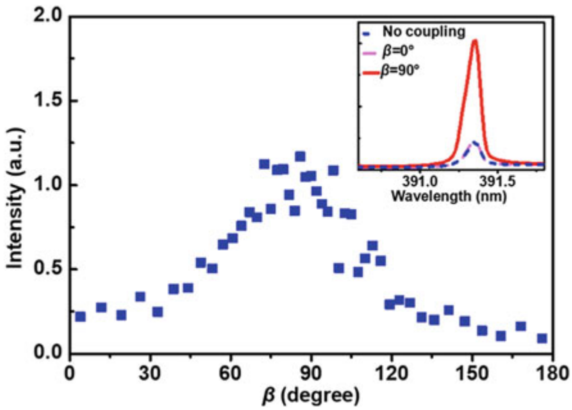

Fig. 2.8 The intensity of the 391.4 nm lasing as a function of β. Inset: The forward lasing spectra obtained in the presence of the coupling field for the cases of $\beta = 0°$ (pink dash) and $\beta = 90°$ (red solid), and that obtained in the absence of the coupling field (blue dash)

the polarization directions of these two pulses are parallel and perpendicular, respectively. In this measurement, the pressure of N_2 gas in the chamber is 10 mbar, and the coupling laser energy is 180 μJ. As an example, the lasing spectra measured at $\beta = 0°$ and $\beta = 90°$ are shown in the inset of Fig. 2.8, where the lasing spectrum in the absence of the coupling pulse is also presented. It can be seen from Fig. 2.8 that the 391.4 nm lasing intensity increases from $\beta = 0°$ to 90°, and the decreases from $\beta = 90°$ to 180°, with the maximum value taking at $\beta \sim 90°$.

This indicates that as the polarization directions of these two pulses are perpendicular, the population in the $X^2\Sigma_g{}^+$ ($\upsilon'' = 0$) can be depleted more efficiently, which is in good agreement with our conjecture that the perpendicular transition between the $X^2\Sigma_g{}^+$ ($\upsilon'' = 0$) and $A^2\Pi_u$ states is sensitive to the polarization direction of the coupling laser, so that the optimized population inversion between the $B^2\Sigma_u{}^+$ (υ = 0) and $X^2\Sigma_g{}^+$ ($\upsilon'' = 0$) states takes place when the polarization direction of the coupling field is set to be perpendicular to that the pump laser pulse, with which the N_2 molecules having the molecular axis parallel to the pump laser polarization are preferentially ionized [30].

Furthermore, since the coupling laser wavelength is resonant with the $X^2\Sigma_g{}^+$ ($\upsilon'' = 0$)-$A^2\Pi_u$ ($\upsilon' = 2$) transition, it is also expected that the efficiency of the post-ionization optical coupling shall be strongly dependent on the intensity of the coupling field. Therefore, we measure in Fig. 2.9 the intensity of the 391.4 nm lasing as a function of the energy of the coupling laser pulse for the two cases of $\beta = 0°$ (red dot) and $\beta = 90°$ (blue rectangle), respectively. It can be clearly seen from Fig. 2.9 that in the case of $\beta = 90°$ the 391.4 nm lasing signal becomes stronger as the energy of the coupling pulse increases, but in the case of $\beta = 0°$ the 391.4 nm lasing signal does not change much as the energy of the coupling pulse varies. That is, as $\beta = 90°$ the 391.4 nm lasing is sensitive to the coupling laser energy, but as $\beta = 0°$ it is reverse. Based on the above results, we conclude that as the polarization directions of the pump and coupling pulses are parallel ($\beta = 0°$) there is almost no coupling

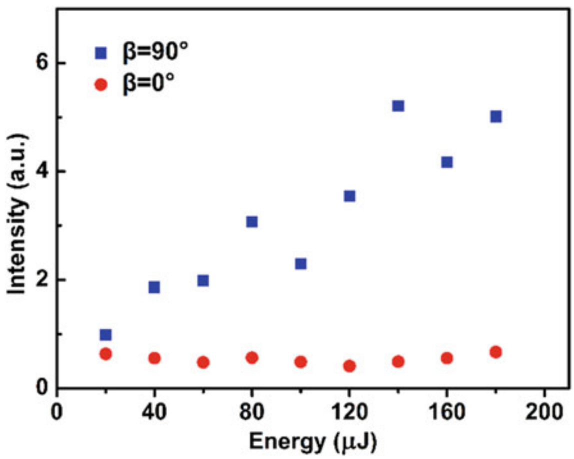

Fig. 2.9 Energy effect of the coupling field on the 391.4 nm lasing intensity for the cases of $\beta = 0°$ (red dot) and $\beta = 90°$ (blue rectangle)

between the $A^2\Pi_u$ ($\upsilon' = 2$) and $X^2\Sigma_g^+$ ($\upsilon'' = 0$) states, but as they are perpendicular, there exists the optical coupling that induce the depletion of the population in the $X^2\Sigma_g^+$ ($\upsilon'' = 0$) state, and thus the variation in the 391.4 nm lasing intensity.

2.3.2 Broadband Few-Cycle Laser Ionization-Coupling Scheme

It is well known that the energy separation information of two levels in an optical transition can be obtained by Fourier transform of its temporal oscillation waveform. Therefore, if when the coupling field is temporally scanned in a pump-probe scheme, one can observe temporal oscillations of N_2^+ lasing with the oscillation frequencies correspond to the $X^2\Sigma_g^+$ ($\upsilon'' = 0$)-$A^2\Pi_u$ (υ') transitions, it would provide a direct evidence for the modulation of the population in the $X^2\Sigma_g^+$ ($\upsilon'' = 0$) state through the optical coupling. To verify this idea, we design a broadband ionization-coupling scheme, in which we employ an intense few-cycle pulse (~7 fs) to induce the ionization of N_2 and generate the self-seed, and a weak few-cycle pulse, whose bandwidth can cover the $X^2\Sigma_g^+$ ($\upsilon'' = 0$)-$A^2{}_u$ ($\upsilon' = 1, 2, 3$) transitions, serves as a coupling field to modulate the population in the $X^2\Sigma_g^+$ ($\upsilon'' = 0$) state [29]. By measuring the intensity of the $B^2\Sigma_u^+$ ($\upsilon = 0$)-$X^2\Sigma_g^+$ ($\upsilon'' = 0$) lasing at 391.4 nm as a function of the pump-probe time delay, we can investigate how the $A^2\Sigma_u$-$X^2\Sigma_g^+$ coupling modulate the lasing temporally.

In Fig. 2.10, we show the dependences of the 391.4 nm lasing intensity on the delay time between the ionization (pump) and the coupling (probe) pulses. Both the ionization and coupling laser pulses are close to linear polarization with the ellipticity of ~0.1. The red and black curves in Fig. 2.10 represent that the time-dependent N_2^+ lasing is measured respectively under the conditions that the polarization directions

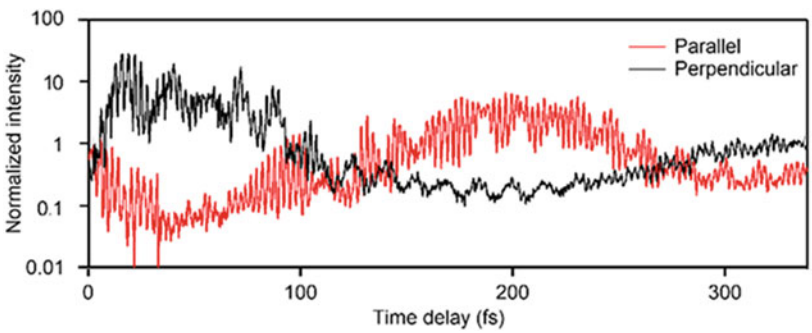

Fig. 2.10 The intensity of 391.4 nm lasing as a function of the time delay between the ionization (pump) and the coupling (probe) pulses measured as the polarization directions of the pump and probe are parallel (red curve) and perpendicular (black curve) to each other. The lasing intensity is normalized by the lasing intensity obtained by the pump laser pulse only

of the ionization and coupling pulses are parallel (red curve) and perpendicular (black curve) with each other. It can be seen from Fig. 2.10 that for both cases the laser intensities oscillate strongly. In the parallel condition, the lasing intensity takes the minimum value at ~20–45 fs and the maximum value at ~200 fs. In the perpendicular case, the lasing intensity takes the maximum value at ~5–45 fs and the minimum value at ~200 fs. At around 15~45 fs, the lasing intensity in the perpendicular condition is ~30 times stronger than that obtained by the pump pulse only, which is consistent with our previous study [26], where we observed ~100 times enhancement of the lasing intensity when we used the polarization modulated pulse whose polarization direction changes by 90° within 20 fs.

In addition, it can be seen from Fig. 2.10 that there is a slow modulation (~300 fs period) of the lasing intensity for both the conditions, which are anti-phased. The slow modulations can be attributed to the field-free rotation motion of N_2^+. The discussion on the contribution of the molecular alignment to the generation of the N_2^+ lasing can be found in [34]. Since the N–N molecular axis of N_2^+ will rotate after ionization, the probability of the perpendicular $X^2\Sigma_g^+$-$A^2\Pi_u$ transition induced by the coupling pulse with the fixed polarization direction will vary as a function of the delay time between the pump and the coupling pulses. As a result, the perpendicular transition of the $X^2\Sigma_g^+$-$A^2\Pi_u$ state effectively enhances the $X^2\Sigma_g^+$-$B^2\Sigma_u^+$ lasing at ~20–45 fs (see black curve) and 200 fs (see red curve). At the delay time of 16 fs, the lasing intensity obtained in the perpendicular case is 300 times larger than that obtained in the parallel case.

It can also be seen in Fig. 2.10 that the lasing intensities for both the parallel and perpendicular conditions exhibit the frequency oscillations with the periods of 2–3 fs, and of 13–20 fs. After the Fourier transform of the lasing oscillations, we obtain the frequency spectra of time-dependent N_2^+ lasing intensity under the (a) parallel and (b) perpendicular conditions, as shown in Fig. 2.11. From the frequency spectra, it can be observed that there are three peaks appearing in the range of 0.3–0.5

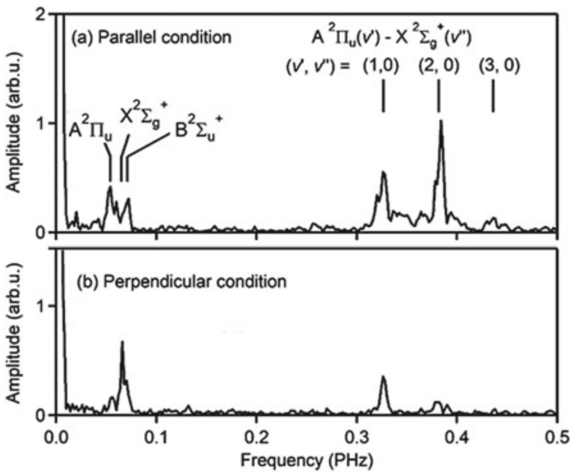

Fig. 2.11 Fourier transform spectra of time-dependent N_2^+ lasing intensity under the **a** parallel and **b** perpendicular conditions

PHz at 0.33, 0.38, and 0.44 PHz in the parallel condition, and two peaks appearing at 0.33 and 0.38 PHz in the perpendicular condition with relatively weak amplitudes. These peaks in the range 0.3–0.5 PHz can be assigned to the energy separations of the ro-vibrational levels between the $A^2\Pi_u$ ($\upsilon' = 1, 2, 3$) and $X^2\Sigma_g{}^+$ ($\upsilon'' = 0$) states. In addition, it can also be seen in Fig. 2.11 that there are peaks at the low frequency range of 0.05–0.08 PHz, which are assigned to the vibrational level separations of the three respective electronic states of $X^2\Sigma_g{}^+$, $A^2\Pi_u$, and $B^2\Sigma_u{}^+$. These results clearly show that the lowest three electronic states in $N_2{}^+$ are coupled coherently by the ionization pulse, resulting in the final modulations in the $B^2\Sigma_u{}^+$-$X^2\Sigma_g{}^+$ lasing by the coupling pulse.

2.4 Optimization of $N_2{}^+$ Lasing by Modulating the Polarization State of the Pump Laser Pulse

So far, we have revealed, based on the above results, that the strong-field-induced $N_2{}^+$ lasing can be convincingly explained by the post-ionization $B^2\Sigma_u{}^+$-$X^2\Sigma_g{}^+$-$A^2\Pi_u$ three-state coupling model. This interpretation will be very helpful for developing a variety of techniques to manipulate and optimize $N_2{}^+$ lasing. In particular, it is known from Sect. 2.2 that within the pump pulse two processes essentially take place to achieve the lasing emission: (i) the preparation of population in the lowest three $X^2\Sigma_g{}^+$, $A^2\Pi_u$ and $B^2\Sigma_u{}^+$ states through the ionization of N_2 by the central (strongest) part of the pulse, and (ii) the modulation of the population in the $X^2\Sigma_g{}^+$ state by the later part of the pulse. Therefore, in the following we will present two examples of optimizing $N_2{}^+$ lasing at 391.4 nm by modifying the relative amplitudes and the temporal separation of the two polarization components in an elliptically modulated ultrashort pulsed laser field.

2.4.1 Optimization of $N_2{}^+$ Lasing Using Different Orders of QWPs

As presented in Sect. 2.2.2, it is found that the 391.4 nm lasing intensity can be significantly enhanced by changing the angle α between the polarization direction of the pump laser pulse and the optical axis of the 7-QWP, which is ascribed to the balance between the ionization rate of N_2 and the coupling efficiency of $N_2{}^+$ induced respectively by the the two polarization components in the elliptically modulated ultrashort pulsed laser field by the 7-QWP. Here we further investigate the optimization of $N_2{}^+$ lasing using different orders of QWPs.

In Fig. 2.12, we present the lasing intensity at 391.4 nm measured with n-QWP in an external seed scheme as a function of the angle α, where n = 0, 3, 7, 10, respectively [27]. It can be seen from Fig. 2.12 that as α changes from 0° to 45°

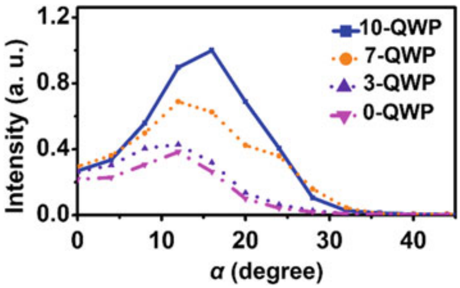

Fig. 2.12 The lasing intensity at 391.4 nm as a function of α with n = 0 (purple downward triangle), 3 (violet upward triangle), 7 (orange dot), 10 (blue rectangle)

the 391.4 nm lasing intensity first increases and then decreases for all the four QWP cases. It can also be noted that the maximum intensity of the 391.4 nm lasing increases monotonically as the order of the QWP increases from $n = 0$ to 10, and that the angle α, at which the lasing intensity becomes maximum, moves from $\alpha \sim 12°$ to $\alpha \sim 18°$.

The optimization of N_2^+ lasing using n-order QWPs can be well understood based on the coupling model due to the balance between the ionization and the coupling induced respectively by the the two polarization components in the elliptically pulsed laser field. As shown in Fig. 2.13, it can be seen that when n increases from 0 to 10, for a certain angle of α, although the relative amplitudes of the two polarization components, E_y and E_x, keep constant, their temporal separation in the pump pulse increases, which means that after the ionization of N_2 by the strongest part of the E_y component, the effective coupling part in the E_x component becomes more due to the more delayed $E_x(t)$ component. This gives rise to the more efficient depletion in the $X^2\Sigma_g^+$ ($\upsilon'' = 0$) state through the $X^2\Sigma_g^+$-$A^2\Pi_u$ vertical transition, leading to the enhanced lasing intensity with increasing n from 0 to 10.

Therefore, the key factor for the optimization of the $B^2\Sigma_u^+$ ($\upsilon = 0$)-$X^2\Sigma_g^+$ ($\upsilon'' =$ 0) lasing is the $E_x(t)$ component of the laser field interacting with N_2^+ in the latter part of the laser field. However, it should be emphasized that although the experimental results shown in Fig. 2.12 demonstrate that the lasing intensity increases as the QWP order increases (up to $n = 10$), there should be an upper limit for the order n when the lasing intensity starts to decrease. Actually, it is estimated that when the order n increases up to about $n = 15$, the two components, E_x and E_y, of the pump laser pulse are separated in time almost completely, and therefore, the lasing signal intensity could not increase more even when the order increases more. Furthermore, if the

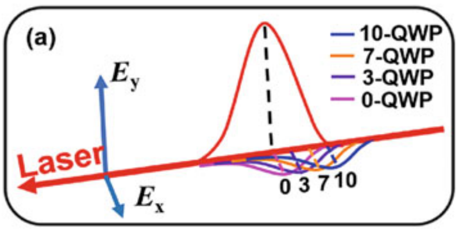

Fig. 2.13 Schematic diagram of the variation in the temporal separation between the two polarization components for the cases of $n = 0, 3, 7, 10$, respectively

order increases further, the intensity of these two components decreases because of the frequency chirp, and consequently, the lasing intensity will start dropping.

2.4.2 Asymmetric Enhancement of N_2^+ Lasing in an Elliptically Modulated Laser Field.

In Sect. 2.4.1, we demonstrate the optimization of N_2^+ lasing at 391.4 nm in an elliptical laser field modulated by *n*-QWPs for the angle α in a small range of α = 0°–45°. Here we demonstrate that when we extend the angle α to a larger angle range of α ~ 0°–90°, an asymmetric enhancement feature of the 391.4 nm lasing is observed, which further shows the effect of the relative amplitudes of the two polarization components on the ionization and coupling in the birefringence-modulated elliptically laser fields [35].

In Fig. 2.14, we plot the intensity of 391.4 nm lasing measured in an external seed scheme as a function of α, in the range of 0°–90° [35]. The N_2 gas pressure is 8 mbar, and the energies of the pump and probe laser pulses are 0.7 mJ and 100 nJ, respectively. It can be seen from Fig. 2.14 that the optimized intensities of the 391.4 nm lasing appear at α ~ 14° and 73° with the ellipticity of $\varepsilon \sim 0.3$, but the lasing enhancement at α ~ 14° is about 3 times larger than that at α ~ 73°, even though the laser pulse at these two positions have almost the same ellipticity value of $\varepsilon \sim 0.3$.

The above asymmetric enhancements of the 391.4-lasing intensity in the α range of 10°–20° and 70°–80° for the 7-QWP case can be ascribed to the different population depletion in the $X^2\Sigma_g{}^+(\upsilon'' = 0)$ due to the different $X^2\Sigma_g{}^+$-$A^2\Pi_u$ coupling contribution provided by the rear laser field after ionization. Based on (2.3), after passing through 7-QWP, the laser pulse is divided into the two polarization components, where when 0° < α < 45° (Fig. 2.15a), the amplitude of $\boldsymbol{E}_\mathbf{y}$ is larger than that of $\boldsymbol{E}_\mathbf{x}$, while when 45° < α < 90° (Fig. 2.15b), the situation is reversed. It can be seen from Fig. 2.15 that when 0° < α < 45° the ionization of N_2 is induced by the yellow part in the stronger component (yellow part) of the pulse, and subsequently, the vertical $X^2\Sigma_g{}^+$-$A^2\Pi_u$ coupling proceeds by the weaker component in the violet

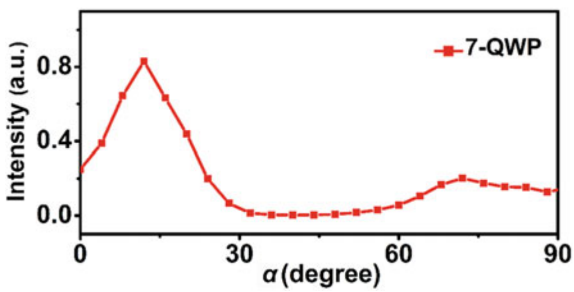

Fig. 2.14 The intensity of the 391.4 nm lasing measured in the 7-QWP modulated laser field as a function of the angle α between the polarization direction of the linearly polarized laser pulse and the fast axis of 7-QWP

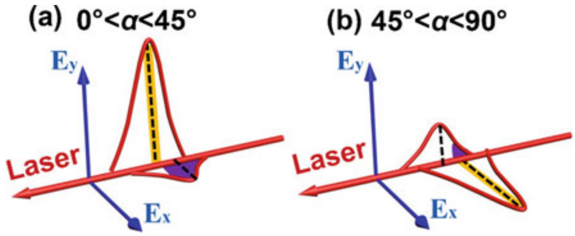

Fig. 2.15 Schematic diagram of the variation in the amplitudes of the two orthogonally-polarized laser components in the 7-QWP modulated laser field with **a** 0° < α < 45° and **b** 45° < α < 90°

region. On the other hand, when 45° < α < 90°, if the ionization process occurs within the stronger component, only a small portion (violet region) of the weaker component of the pulse can contribute to the coupling process. Therefore, even though the laser fields in the two α ranges shown in Fig. 2.15a and b have the same ellipticity, the relative amplitudes of E_x and E_y is opposite in the two cases, leading to the different strengths of the $X^2\Sigma_g{}^+$-$A^2\Pi_u$ coupling after the ionization of N_2, and thus the different 391.4 nm lasing intensities.

2.5 Summary

In summary, we have investigated the $N_2{}^+$ lasing actions induced by intense laser fields, and presented indirect and direct experimental evidences for the post-ionization optical coupling in $N_2{}^+$ in intense laser fields by modulating the polarization state of the pump pulse, as well as by using pump-probe methods. We demonstrated that the $N_2{}^+$ lasing at 391.4 nm, corresponding to the $B^2\Sigma_u{}^+$ ($\upsilon = 0$)-$X^2\Sigma_g{}^+$ ($\upsilon'' = 0$) transition, is strongly sensitive to the polarization state of the rear part of the pump laser pulse, and contributed it to the efficient population transfer from the ground $X^2\Sigma_g{}^+$ ($\upsilon'' = 0$) state to the first excited $A^2\Pi_u$ state of $N_2{}^+$.

By using pump-probe methods, we further showed that the vertical transition between the $X_2\Sigma_g{}^+$ and $A^2\Pi_u$ states of $N_2{}^+$ are sensitive to the polarization direction and the energy of the resonant coupling pulse. In addition, by introducing the broadband coupling pulse, we were able to show the optical transitions between different vibrational levels of the $X^2\Sigma_g{}^+$ and $A^2\Pi_u$ states by Fourier transforms of the lasing intensity oscillations observed in the temporal domain.

With the knowledge of the balance between the ionization of N_2 and the coupling of $N_2{}^+$ in the elliptically polarized pulse, we showed the optimization of $N_2{}^+$ lasing at 391.4 nm by changing the temporal separation between the two perpendicular polarization components and their relative amplitudes by using multi-order QWPs. We also revealed that the $N_2{}^+$ lasing at 427.8 nm, corresponding to the $B^2\Sigma_u{}^+$ ($\upsilon = 0$)-$X^2\Sigma_g{}^+$ ($\upsilon'' = 0$) transition, cannot be well manipulated by modulating the polarization state of the rear part of the laser pulse. We have convincingly explained the different ellipticity dependence on the two $N_2{}^+$ lasing lines at 391.4 and 427.8 nm by the post-ionization coupling model.

The results presented in this chapter provide reliable evidences for understanding the N_2^+ lasing mechanism, based which the optimization of intense N_2^+ lasing can be realized, which will benefit for the promising application of air lasing in a variety of fields such as remote sensing and standoff spectroscopy.

Acknowledgements The work is supported in part by National Natural Science Foundation of China (NSFC) (61625501, 61427816) and by the two MEXT (Ministry of Education, Culture, Sports, Science and Technology) Grant-in-Aid for Specially Promoted Research (#19002006 and #15H05696).

References

1. A.L. Gaeta, Catastrophic collapse of ultrashort pulses. Phys. Rev. Lett. **84**, 3582 (2000). https://doi.org/10.1103/physrevlett.84.3582
2. H.L. Xu, A. Azarm, J. Bernhardt, Y. Kamali, S.L. Chin, The mechanism of nitrogen fluorescence inside a femtosecond laser filament in air. Chem. Phys. **360**, 171 (2009). https://doi.org/10.1016/j.chemphys.2009.05.001
3. J.L. Liu, J.M. Dai, S.L. Chin, X.C. Zhang, Broadband terahertz wave remote sensing using coherent manipulation of fluorescence from asymmetrically ionized gases. Nat. Photon. **4**, 627 (2010). https://doi.org/10.1038/nphoton.2010.165
4. H.L. Xu, S.L. Chin, Femtosecond laser filamentation for atmospheric sensing. Sensors **11**, 32 (2011). https://doi.org/10.3390/s110100032
5. Q. Luo, W. Liu, S.L. Chin, Lasing action in air induced by ultra-fast laser filamentation. Appl. Phys. B **76**, 337–340 (2003). https://doi.org/10.1007/s00340-003-1115-9
6. W. Chu, B. Zeng, J. Yao, H. Xu, J. Ni, G. Li, H. Zhang, F. He, C. Jing, Y. Cheng, Z. Xu, Multiwavelength amplified harmonic emissions from carbon dioxide pumped by mid-infrared femtosecond laser pulses. EPL—Europhys. Lett. **97**, 64004 (2012). https://doi.org/10.1209/0295-5075/97/64004
7. S. Yuan, T.J. Wang, Y. Teranishi, A. Sridharan, S.H. Lin, H.P. Zeng, S.L. Chin, Lasing action in water vapor induced by ultrashort laser filamentation. Appl. Phys. Lett. **102**, 224102 (2013). https://doi.org/10.1063/1.4809585
8. A. Dogariu, J.B. Michael, M O. Scully, R.B. Miles, High-gain backward lasing in air. Science **331**, 442-445 (2011). https://doi.org/10.1126/science.1199492
9. A. Laurain, M. Scheller, P. Polynkin, Low-threshold bidirectional air lasing. Phys. Rev. Lett. **113**, 253901 (2014). https://doi.org/10.1103/PhysRevLett.113.253901
10. D. Kartashov, S. Ališauskas, A. Baltuška, A. Schmitt-Sody, W. Roach, P. Polynkin, Remotely pumped stimulated emission at 337 nm in atmospheric nitrogen. Phys. Rev. A **88**, 041805 (2013). https://doi.org/10.1103/PhysRevA.88.041805
11. S. Mitryukovskiy, Y. Liu, P. Ding, A. Houard, A. Mysyrowicz, Backward stimulated radiation from filaments in nitrogen gas and air pumped by circularly polarized 800 nm femtosecond laser pulses. Opt. Express **22**, 12750–12759 (2014). https://doi.org/10.1364/OE.22.012750
12. J. Yao, H. Xie, B. Zeng, W. Chu, G. Li, J. Ni, H. Zhang, C. Jing, C. Zhang, H. Xu, Y. Cheng, Z. Xu, Gain dynamics of a free-space nitrogen laser pumped by circularly polarized femtosecond laser pulses. Opt. Express **22**, 19005–19013 (2014). https://doi.org/10.1364/OE.22.019005
13. J. Ni, W. Chu, H. Zhang, C. Jing, J. Yao, H. Xu, B. Zeng, G. Li, C. Zhang, S. Chin, Y. Cheng, Z. Xu, Harmonic-seeded remote laser emissions in N2-Ar, N2-Xe and N2-Ne mixtures: a comparative study. Opt. Express **20**, 20970–20979 (2012). https://doi.org/10.1364/OE.20.020970

14. J. Yao, B. Zeng, H. Xu, G. Li, W. Chu, J. Ni, H. Zhang, S. L. Chin, Y. Cheng, Z. Xu, High-brightness switchable multiwavelength remote laser in air. Phys. Rev. A **84**, 051802 (2011). https://doi.org/10.1103/PhysRevA.84.051802
15. H. Li, D. Yao, S. Wang, Y. Fu, H. Xu, Air lasing: phenomena and mechanisms. Chin. Phys. B **28**, 114204 (2019). https://doi.org/10.1088/1674-1056/ab47f5
16. H. Zhang, C. Jing, J. Yao, G. Li, B. Zeng, W. Chu, J. Ni, H. Xie, H. Xu, S. L. Chin, K. Yamanouchi, Y. Cheng, Z. Xu, Rotational coherence encoded in an "air-laser" spectrum of nitrogen molecular ions in an intense laser field. Phys. Rev. X **3**, 041009 (2013). https://doi.org/10.1103/PhysRevX.3.041009
17. Z. Liu, J. Yao, H. Zhang, B. Xu, J. Chen, F. Zhang, Z. Zhang, Y. Wan, W. Chu, Z. Wang, Y. Cheng, Extremely nonlinear Raman interaction of an ultrashort nitrogen ion laser with an impulsively excited molecular wave packet. Phys. Rev. A **101**, 043404 (2020). https://doi.org/10.1103/PhysRevA.101.043404
18. P.R. Hemmer, R.B. Miles, P. Polynkin, T. Siebert, A.V. Sokolov, P. Sprangle, M.O. Scully, Standoff spectroscopy via remote generation of a backward-propagating laser beam. Proc. Nat. Acad. Sci. USA **108**, 3130 (2011). https://doi.org/10.1073/pnas.1014401107
19. G. Herzberg, Molecular spectra and molecular structure. I. spectra of diatomic molecules. Am. J. Phys. **19**, 390(1951). https://doi.org/10.1119/1.1932852
20. A. Becker, A.D. Bandrauk, S.L. Chin, S-matrix analysis of non-resonant multiphoton ionisation of inner-valence electrons of the nitrogen molecule. Chem. Phys. Lett. **343**, 345–350 (2001). https://doi.org/10.1016/s0009-2614(01)00705-9
21. S.F. Zhao, C. Jin, A.T. Le, T.F. Jiang, C.D. Lin, Determination of structure parameters in strong-field tunneling ionization theory of molecules. Phys. Rev. A, 82, 049903 (2010) (Phys. Rev. A **81**, 033423 (2010)). https://doi.org/10.1103/PhysRevA.82.049903
22. A. Azarm, P. Corkum, P. Polynkin, Optical gain in rotationally excited nitrogen molecular ions. Phys. Rev. A **96**, 051401 (2017). https://doi.org/10.1103/PhysRevA.96.051401
23. Y. Liu, P. Ding, G. Lambert, A. Houard, V. Tikhonchuk, A. Mysyrowicz, Recollision-induced superradiance of ionized nitrogen molecules. Phys. Rev. Lett. **115**, 133203 (2015). https://doi.org/10.1103/PhysRevLett.115.133203
24. J. Yao, S. Jiang, W. Chu, B. Zeng, C. Wu, R. Lu, Z. Li, H. Xie, G. Li, C. Yu, Z. Wang, H. Jiang, Q. Gong, Y. Cheng, Population redistribution among multiple electronic states of molecular nitrogenions in strong laser fields. Phys. Rev. Lett. **116**, 143007 (2016). https://doi.org/10.1103/PhysRevLett.116.143007
25. H. Xu, E. Lötstedt, A. Iwasaki, K. Yamanouchi, Sub-10-fs population inversion in N2+ in air lasing through multiple state coupling. Nat. Commun. **6**, 8347 (2015). https://doi.org/10.1038/ncomms9347
26. H. Li, M. Hou, H. Zang, Y. Fu, E. Lötstedt, T. Ando, A. Iwasaki, K. Yamanouchi, H. Xu, Significant enhancement of N_2^+ lasing by polarization-modulated ultrashort laser pulses. Phys. Rev. Lett. **122**, 013202 (2019). https://doi.org/10.1103/PhysRevLett.122.013202
27. Y. Fu, E. Lötstedt, H. Li, S. Wang, D. Yao, T. Ando, A. Iwasaki, F.H.M. Faisal, K. Yamanouchi, H. Xu, Optimization of N_2^+ lasing through population depletion in the $X^2\Sigma_g^+$ state using elliptically-modulated ultrashort intense laser fields. Phys. Rev. R. **2**, 012007(R) (2020). https://doi.org/10.1103/PhysRevResearch.2.012007
28. S. Wang, Y. Fu, D. Yao, S. Chen, W. Zhang, H. Li, H. Xu, Observation of the optical $X^2\Sigma_g^+ - A^2\Pi_u$ coupling in N_2^+ lasing induced by intense laser field. Chin. Phys. B **28**, 123301 (2019). https://doi.org/10.1088/1674-1056/ab54b1
29. T. Ando, E. Lötstedt, A. Iwasaki, H. Li, Y. Fu, S. Wang, H. Xu, K. Yamanouchi, Rotational, vibrational, and electronic modulations in N_2^+ lasing at 391.4 nm: evidence of coherent $B^2\Sigma_u^+ - X^2\Sigma_g^+ - A^2\Pi_u$ coupling. Phys. Rev. Lett. **123**, 203201 (2019). https://doi.org/10.1103/PhysRevLett.123.203201
30. D. Pavičić, K.F. Lee, D.M. Rayner, P.B. Corkum, D.M. Villeneuve, Direct measurement of the angular dependence of ionization for N_2, O_2, and CO_2 in intense laser fields. Phys. Rev. Lett. **98**, 243001 (2007). https://doi.org/10.1103/PhysRevLett.98.243001

31. S.R. Langhoff, Jr C.W. Bauschlicher, H. Partridge, Theoretical study of the N_2^+ Meinel system. J. Chem. Phys. **87**, 4716 (1987). https://doi.org/10.1063/1.452835
32. Z.H. Chang, Single attosecond pulse and xuv supercontinuum in the high-order harmonic plateau. Phys. Rev. A **70**, 043802 (2004). https://doi.org/10.1103/physreva.70.043802
33. F.R. Gilmore, R.R. Laher, P.J. Espy, Franck–Condon factors, r-centroids, electronic transition moments, and Einstein coefficients for many nitrogen and oxygen band systems. J. Phys. Chem. Ref. Data **21**, 1005–1107 (1992). https://doi.org/10.1063/1.555910
34. H. Xu, E. Lötstedt, T. Ando, A. Iwasaki, K. Yamanouchi, Alignment-dependent population inversion in N_2^+ in intense few-cycle laser fields. Phys. Rev. A **96**, 041401 (2017). https://doi.org/10.1103/PhysRevA.96.041401
35. Y. Fu, S. Chen, S. Wang, W. Zhang, D. Yao, H. Zang, H. Li, H. Xu, Asymmetric enhancement of N_2^+ lasing in intense, birefringence-modulating elliptical laser fields. Opt. Express **28**, 23274–23283 (2020). https://doi.org/10.1364/OE.389284